https://doi.org/10.5194/egusphere-2025-4864
Preprint. Discussion started: 7 October 2025
© Author(s) 2025. CC BY 4.0 License.

A hybrid optimal estimation and machine learning approach to predict atmospheric composition

Frank Werner[1], Kevin W. Bowman[1], Seungwon Lee[1], Joshua L. Laughner[1], Vivienne H. Payne[1], and James L. McDuffie[1]

[1]Jet Propulsion Laboratory, California Institute of Technology, 4800 Oak Grove Drive, Pasadena, CA 91109, USA

Correspondence: Frank Werner (frank.werner@jpl.nasa.gov)

Abstract. We present a HYbrid REtrieval Framework (HYREF) that predicts subcolumn carbon monoxide (CO) concentrations from Cross-track Infrared Sounder (CrIS) observations, trained to replicate the TRopospheric Ozone and its Precursors from Earth System Sounding (TROPESS) retrievals based on optimal estimation (OE). Unlike the OE algorithm, which produces retrievals for only a small fraction of available CrIS observations due to expensive but physically accurate radiative transfer, the addition of machine learning (ML) techniques enables full coverage by providing high–resolution predictions for every valid CrIS sample. Importantly, in addition to CO concentrations, TROPESS–HYREF also predicts key retrieval diagnostics, namely column averaging kernels, degrees of freedom, and retrieval errors, that are essential for meaningful comparison with other observations, models, and ingestion into data assimilation.

The new framework achieves excellent performance with correlation coefficients $r > 0.99$ and a bias $< 0.1\%$ when benchmarked against an independent test set, and reproduces fine–scale spatial patterns in CO fields observed during a major wildfire over North America. A scale analysis reveals substantial variability in CO concentrations below the nominal $0.80°$ resolution of the TROPESS OE retrieval, which TROPESS–HYREF successfully resolves. Inference is computationally efficient, with daily global predictions completed in minutes on a single compute node. Continuous training with the operational TROPESS OE algorithm ensures that TROPESS–HYREF adapts to changes in the trends and variability of atmospheric composition. This threading of OE–derived physical information and ML–driven efficiency provides a practical pathway to high–resolution atmospheric CO monitoring with robust diagnostics.

Copyright statement. ©2025. California Institute of Technology.

1 Introduction

Carbon monoxide (CO) is a chemically reactive trace gas and key atmospheric pollutant, produced primarily through incomplete combustion of biomass and fossil fuels (Jacob, 1999), as well as through secondary production from the oxidation of methane (CH_4) and non–methane hydrocarbons (e.g., Holloway et al., 2000). It plays a central role in atmospheric chemistry by serving as a major sink for hydroxyl radicals (OH, Lelieveld et al., 2016), thereby influencing the oxidative capacity of the

https://doi.org/10.5194/egusphere-2025-4864
Preprint. Discussion started: 7 October 2025
© Author(s) 2025. CC BY 4.0 License.

atmosphere and the lifetime of CH_4 (e.g., Gaubert et al., 2017). Due to its intermediate lifetime (weeks to months), CO serves as a valuable tracer for long–range pollution transport and chemical processing in the troposphere (e.g., Clerbaux et al., 2002; Edwards et al., 2004). It also contributes indirectly to radiative forcing via the formation of tropospheric ozone (O_3) and carbon dioxide (CO_2), classifying it as a short-lived climate pollutant (Bowman and Henze, 2012; IPCC, 2023).

Satellite observations of CO, beginning with the Measurements of Air Pollution from Satellites (MAPS, Reichle Jr. et al., 1990) in the early 1980s and continuing with instruments such as Measurement of Pollution in the Troposphere (MOPITT) (Drummond et al., 2010), Atmospheric Infrared Sounder (AIRS) (Aumann et al., 2003), Tropospheric Emission Spectrometer (TES) (Beer et al., 2001), Infrared Atmospheric Sounding Interferometer (IASI) (Clerbaux et al., 2009), Cross–track Infrared Sounder (CrIS) (Han et al., 2013), TROPOspheric Monitoring Instrument (TROPOMI) (Veefkind et al., 2012), Greenhouse Gases Observing Satellite 2 (GOSAT–2) (Noël et al., 2022) and Geostationary Interferometric Infrared Sounder (GIIRS) (Zeng et al., 2023), have provided a long–term, global perspective on CO distributions, emission sources, and trends (e.g., Worden et al., 2013; Buchholz et al., 2021). These datasets support air quality monitoring, inverse modeling of emissions, and evaluation of chemistry-climate models (e.g., Field et al., 2015, 2016; Buchholz et al., 2018). While global CO concentrations have declined over the past two decades due to improved combustion efficiency and decreased biomass burning (e.g., Schultz et al., 2015; Zheng et al., 2019), recent regional fire trends (see, e.g., Luo et al. 2024), and evolving air quality policies continue to shape CO variability, underscoring the need for sustained satellite observations with well–characterized uncertainties (e.g., Strode et al., 2016). Nevertheless, changes in climate and extreme events can lead to substantial biomass burning events for which CO is a critical tracer to infer emissions (Byrne et al., 2021, 2024; Neyra-Nazarrett et al., 2025).

The NASA TRopospheric Ozone and its Precursors from Earth System Sounding (TROPESS) project generates consistent, long-term records of tropospheric ozone and related trace gases, including CO (Bowman, 2021; Worden et al., 2022). Building on the TES legacy, TROPESS applies a unified optimal estimation (OE, see, e.g., Rodgers 2000) algorithm across multiple satellite platforms, supported by a comprehensive ground data system (Bowman et al., 2006; Fu et al., 2016). Emphasis is placed on rigorous uncertainty analysis and intercomparisons with independent observations to ensure the accuracy needed for trend detection. Figure 1a shows the spatial distribution of operational TROPESS Level 2 (L2) CO retrievals over the western United States on 10 June 2023, based on CrIS measurements. A regional zoom (red box) reveals that, due to computational constraints, only $\approx 1.5\%$ of the available CrIS soundings are processed, leaving substantial gaps in global CO monitoring.

Machine learning (ML) approaches, whose use in atmospheric science has expanded in recent years (e.g., Grivas and Chaloulakou, 2006; Saponaro et al., 2013; Werner et al., 2020; Schultz et al., 2021; Werner et al., 2023), offer a promising path forward. ML models can efficiently learn complex, nonlinear relationships and provide rapid inference across large datasets. However, limitations in explainability and uncertainty quantification continue to hinder their broader application in remote sensing (Tyralis and Papacharalampous, 2024).

In contrast to conventional OE retrievals, which produce not only the retrieved quantities of interest but also key diagnostics, such as χ^2 statistics, degrees of freedom (DoF), retrieval precision, error covariance, and averaging kernels, ML methods lack direct analogues to these quantities. Yet such diagnostics are critical for model–observation comparisons, data assimilation, and quality control (Jones et al., 2003; Miyazaki et al., 2015; von Clarmann and Glatthor, 2019).

https://doi.org/10.5194/egusphere-2025-4864
Preprint. Discussion started: 7 October 2025
© Author(s) 2025. CC BY 4.0 License.

Here, we present a novel hybrid framework that combines the strengths of OE and ML to generate high–resolution estimates of CO column concentrations from CrIS radiances. Our approach leverages OE retrievals both as training targets and as sources of physically meaningful priors, while also enabling ML–driven enhancements such as rapid upscaling and the emulation of retrieval diagnostics. This fusion of the two concepts not only fills in observational gaps left by current processing limits, but also provides an interpretable, uncertainty–aware pathway for incorporating ML into operational remote sensing pipelines.

2 Data

The CrIS instrument, onboard NOAA's Joint Polar Satellite System–1 (JPSS–1, also known as NOAA-20), is a Fourier Transform Spectrometer that captures Earth views across 30 cross–track interferograms, providing a swath width of 2,200 km. Each interferogram contains a 3×3 array of fields of view (FOVs), with each circular FOV having a diameter of 14 km at nadir. CrIS data are processed to provide calibrated Level 1B (L1B) radiances in three spectral bands: 660–1095 cm^{-1} (longwave), 1210–1750 cm^{-1} (midwave), and 2155–2550 cm^{-1} (shortwave). The instrument unapodized spectral resolution is 0.625–2.5 cm^{-1}. NASA's version 2 L1B radiances are available from the Goddard Earth Sciences Data and Information Services Center (GES DISC) UW-Madison Space Science and Engineering Center: Hank Revercomb; UMBC Atmospheric Spectroscopy Laboratory: Larrabee Strow, 2018.

TROPESS trace gas retrievals are provided on a reduced horizontal grid of $0.8°$ by the MUSES data processing system (Fu et al., 2016, 2018, 2019). These retrievals are based on the TES L2 processing algorithm (Bowman et al., 2006) and utilize an OE retrieval approach (Rodgers, 2000). TROPESS retrievals of carbon monoxide (CO) are processed operationally, have undergone extensive verification (e.g., Worden et al., 2022; Luo et al., 2024), and are accessible via the GES DISC. In this study, single–FOV CrIS–MUSES retrievals from the TROPESS forward stream were used (Bowman, 2021).

3 ML model

3.1 Setup and training

We developed, trained, and evaluated a ML model to simultaneously predict a variety of TROPESS CO variables, primarily using observed CrIS radiances and geolocation data as inputs. This setup is illustrated in the simplified diagram in Fig. 1b, where we drastically limit the input and output variables to aid visibility. In this example the model uses three features ($\mathbf{F}_{1-3}$) as input: CrIS radiances at 2,181.88 cm^{-1}, the sensor viewing angle, and the surface altitude, respectively. These features are matrices, where each element f^s_{1-3} corresponds to one of the N samples, indexed as $s = 1, \ldots, N$. The ML model maps these features to a set of output labels ($\mathbf{L}_{1-3}$), which in this simplified example are the CO total column concentrations, the total column retrieval error, and the column averaging kernel at ≈ 511 hPa. Like the features, these labels are matrices that contain elements l^s_{1-3} for each individual sample. Again, $s = 1, \ldots, N$ denotes the individual sample (i.e., CrIS column).

The ML model developed in this study is a feedforward artificial neural network (ANN), which maps the input to the output through several hidden layers, each consisting of a large number of interconnected neurons. A simplified schematic of

https://doi.org/10.5194/egusphere-2025-4864
Preprint. Discussion started: 7 October 2025
© Author(s) 2025. CC BY 4.0 License.

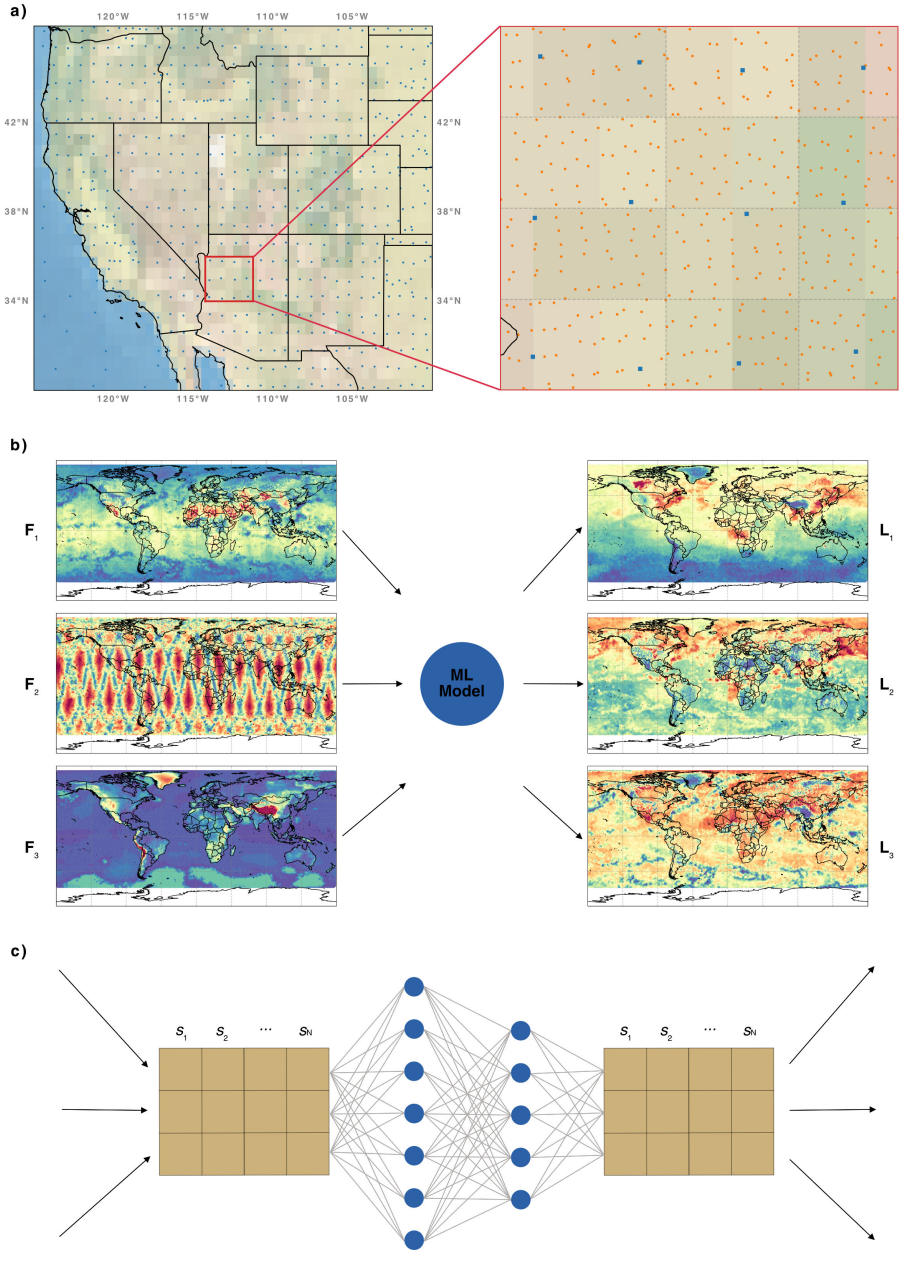

Figure 1. (a) Geolocations of L2 CO retrievals (blue dots) and L1B CrIS radiances (orange dots) over the western United States on 10 June 2023. (b) Simplified sketch of the ML setup, where three features ($\mathbf{F}_{1-3}$; radiances at 2,181.88 cm^{-1}, sensor viewing angle, and surface altitude) are used as input for the ML model in order to predict three labels ($\mathbf{L}_{1-3}$; CO concentrations, retrieval error, and an individual column averaging kernel). (c) Simplified sketch of the ML model. The variables $\mathbf{F}_{1-3}$ are converted to a two–dimensional input matrix which connects to neurons in two hidden layers, and map to a two–dimensional output matrix, which provides $\mathbf{L}_{1-3}$.

https://doi.org/10.5194/egusphere-2025-4864
Preprint. Discussion started: 7 October 2025
© Author(s) 2025. CC BY 4.0 License.

an example ANN, with two hidden layers containing 7 and 5 neurons, respectively, is shown in Fig. 1c. This diagram also illustrates how the geolocated features are transformed into two–dimensional input and output matrices and how they connect to the individual neurons.

The exact model structure and hyperparameters (i.e., model settings) are determined through the procedures described in Werner et al. (2021, 2023). By applying k–fold cross–validation across a range of potential model setups, the ideal hyperparameters were found to be two hidden layers with 1506 neurons per layer, “Rectified Linear Unit" activation functions after each hidden layer, an L2 weight decay parameter of 5^{-34}, and the “Adaptive Moment Estimation" optimizer with a learning rate of $1e^{-5}$. The loss function minimized during training is the mean squared error. For each training iteration, batches of training samples are passed through the model for both the forward and backward passes; each mini–batch contains 8,192 samples. Further details on these parameters and their impacts are provided in Reed and Marks (1999); Goodfellow et al. (2016); Werner et al. (2021).

Model training was carried out using the “Keras" library for Python (version 2.10.0; Chollet et al., 2015), with “TensorFlow" (version 2.10.0) as the backend (Abadi et al., 2016). Of the available CrIS radiances and TROPESS retrievals over 04/2023–01/2025, 98% of randomly selected samples were used as training data. After each training iteration, the model’s performance was evaluated for an independent validation dataset comprised of 1% of the available data (approximately 185,000 samples). After several thousand iterations, the model weights corresponding to the best performance scores on the validation set were saved.

The specific features used for the CO model include radiances from all 2,224 spectral channels, the FOV index, the latitude and longitude of each sample, UTC time, a day/night flag, the sensor viewing angle, the day of the year, and the TROPESS subcolumn a priori values. This yields an input matrix containing 2,235 variables. Note that the surface altitude was included for models predicting retrievals and diagnostics for other TROPESS species. The predicted labels of the CO model consist of the subcolumn concentrations, column averaging kernels, and subcolumn retrieval errors, resulting in an output matrix containing 24 variables. Model training was performed on a high–performance computing cluster and took ≈ 10 days to converge to a solution for the $> 12,000,000$ model weights.

3.2 Evaluation

Model performance is evaluated using an independent test dataset, which consists of the remaining 1% of randomly sampled data that were not included in the training or validation process. Ideally, (i) the model should reliably predict CO concentration retrievals and OE diagnostics for these data points, even though the ML algorithm was not trained on them, and (ii) performance metrics should be similar to those derived from the training and validation datasets.

Figure 2a presents a joint histogram of total column CO from the ML and OE algorithms for over 180,000 samples in the test dataset. Yellow colors represent regions with the highest density of data points, while blue colors correspond to areas with very few samples. The good agreement between the ML and OE results is evident, as most observations are narrowly clustered around the 1:1 line. Five performance metrics are provided in the panel: Pearson’s product–moment correlation coefficient (r), the root–mean–square deviation ($\sqrt{\Delta^2}$), the median deviation between the predicted and retrieved CO (50p, i.e., the bias), and

https://doi.org/10.5194/egusphere-2025-4864
Preprint. Discussion started: 7 October 2025
© Author(s) 2025. CC BY 4.0 License.

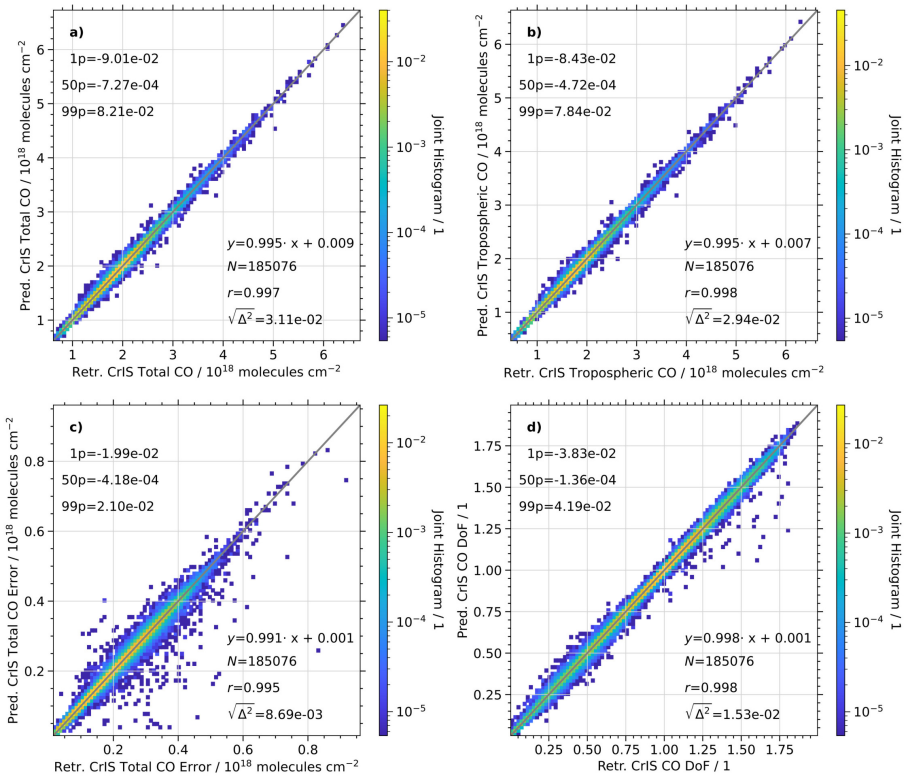

Figure 2. (a) Joint histogram of predicted and retrieved total column CO concentrations from an independent test data set. The gray diagonal line indicates 1:1 correlation. Basic performance metrics for the comparison between ML and OE results are reported in the panel, as well as the linear regression coefficients. (b)–(d) Similar to (a), but for tropospheric column CO concentrations, total column CO retrieval error, and degrees of freedom (DoF).

the 1$^{\mathrm{st}}$ and 99$^{\mathrm{th}}$ percentiles of the deviation. Notably, for the total column concentrations, we find $r > 0.99$, $\sqrt{\Delta^2} = 3.11 \times 10^{16}$ molecules cm^{-2}, a median difference of -7.27×10^{14} molecules cm^{-2}, and maximum absolute differences for the majority of samples of $< 1.00 \times 10^{17}$ molecules cm^{-2}.

Similar comparisons for tropospheric column concentrations, total column retrieval error, and DoF are shown in Figs. 2b–d. Again, the distributions closely follows the 1:1 line, with similarly high correlations ($r > 0.99$). The lowest correlation occurs for the averaging kernel at the lowest atmospheric level (not shown), where $r = 0.98$. These performance metrics are almost identical to those obtained for the validation dataset, where the comparison of predicted and retrieved total column CO concentrations yields $r > 0.99$, $\sqrt{\Delta^2} = 3.14 \times 10^{16}$ molecules cm^{-2}, a median difference of 6.57×10^{14} molecules cm^{-2}, and maximum absolute differences for the majority of samples of $< 1.00 \times 10^{17}$ molecules cm^{-2}.

These results indicate that the trained ML model can reliably replicate the OE subcolumn concentrations and retrieval diagnostics.

https://doi.org/10.5194/egusphere-2025-4864
Preprint. Discussion started: 7 October 2025
© Author(s) 2025. CC BY 4.0 License.

4 Results

4.1 Example maps

Figure 3a presents a representative example scene of total column CO from the TROPESS OE retrieval on 10 June 2023. A large area of enhanced CO concentrations ($> 3 \times 10^{18}$ molecules cm^{-2}) is evident over Western Canada, associated with the unprecedented wildfire season that year (Jain et al., 2024). These fires produced large smoke plumes that affected portions of Canada and the United States for several weeks, before spreading across the Northern Hemisphere. Notably, enhanced CO concentrations ($> 2.5 \times 10^{18}$ molecules cm^{-2}) are also recorded over Eastern Canada, the entire Eastern United States, and parts of the Atlantic Ocean.

The associated OE DoF are shown in Fig. 3b. Areas of moderate to high CO concentrations generally coincide with regions of elevated DoF. Smaller DoF< 0.6 are observed over Greenland, the Atlantic Ocean, and over isolated regions over the continental United States. These reduced DoF are indicative of lower retrieval sensitivity and are likely due to the interference of clouds or poor thermal contrast.

Figures 3c–d show the ML predictions for total CO concentrations and DoF, respectively. These results are derived for each CrIS L1B sample. The increased spatial resolution is particularly noticeable over the oceans, but even over land the ML results capture much finer spatial features, while faithfully reproducing the CO enhancements and DoF from the OE retrieval. Divergence maps in Figs. 3e–f illustrate the differences between predicted and retrieved results. The median differences are $< 0.1\%$ for both variables, and for the majority of samples (i.e., within the 5$^{\text{th}}$ and 95$^{\text{th}}$ percentiles), ML predictions are within $\pm 2.40\%$ for total CO concentrations and within $\pm 4.12\%$ for DoF. Overall, the difference between ML and OE total column CO concentrations exceeds the retrieval error for only 14 of the 5,308 samples in the scene (0.26%). Similarly, excellent agreement is observed for the retrieval errors (not shown), with a majority of ML predictions within $\pm 6.11\%$ and a median difference of 0.04%.

These results demonstrate the ability of the ML model to replicate the OE CO retrievals and diagnostics, while resolving finer spatial features. This quality may enhance the interpretation of observed atmospheric structures.

4.2 The added value from CO at higher spatial resolution

The higher spatial coverage afforded by the algorithm can provide greater insight into the spatial distribution of CO than can be obtained with the nominal $0.80°$ resolution of the TROPESS retrievals. We investigate this advantage through two approaches: (i) comparing the ML–predicted CO fields with linearly interpolated TROPESS CO retrievals, and (ii) performing a scale analysis via the calculation of power spectral densities $E_{\text{I}}(k)$ to look for scale–breaks, especially in the sub–$0.80°$ domain. Each of these methods provides a distinct perspective on the spatial variability in the observed CO fields and whether this variability persists below the operational TROPESS retrieval resolution.

To compute $E_{\text{I}}(k)$, the ML–predicted CO concentrations are interpolated onto a regular grid with constant spacing. As in the previous section, we focus on the total column CO field over North America on 10 June 2023, gridded at a resolution of $0.80°/6 \approx 0.133°$ in both latitude and longitude. Since the CrIS L1B radiances and corresponding ML predictions are provided

https://doi.org/10.5194/egusphere-2025-4864
Preprint. Discussion started: 7 October 2025
© Author(s) 2025. CC BY 4.0 License.

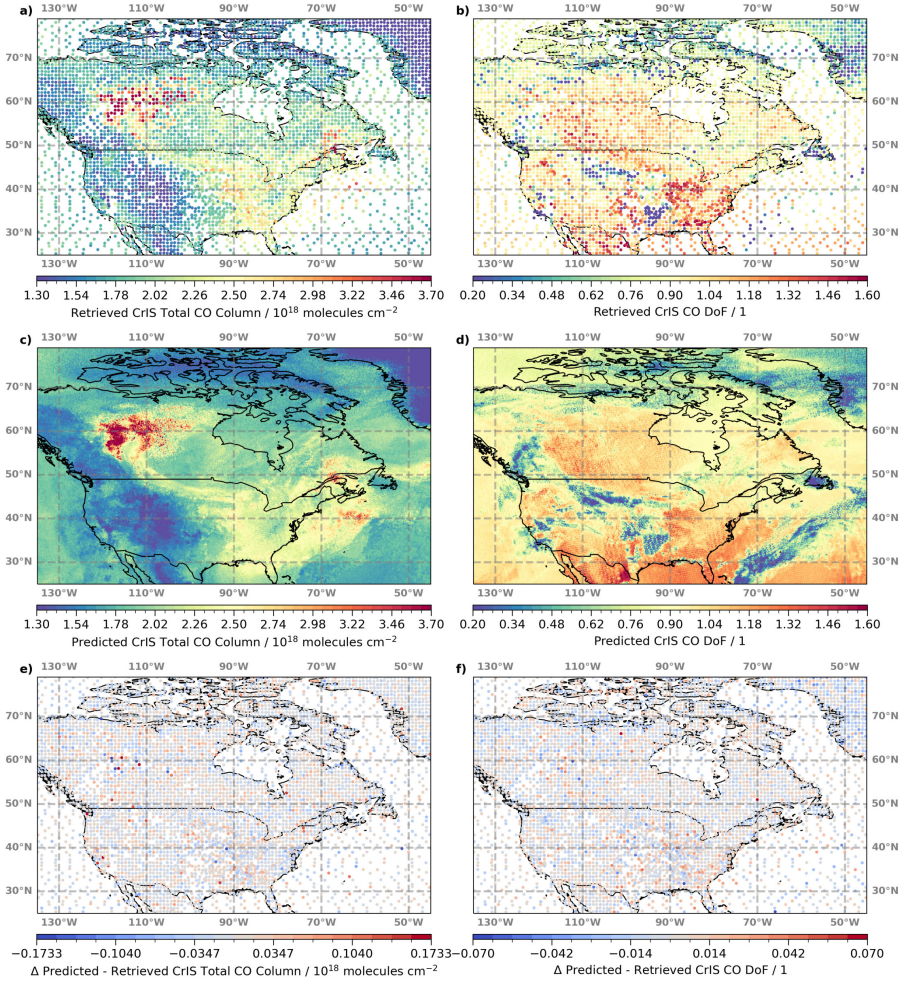

Figure 3. (a) Example scene of OE retrievals of total column CO over North America on 10 June 2023. (b) Similar to (a), but showing the associated OE degrees of freedom (DoF). (c)–(d) Similar to (a)–(b). but for the ML predictions. (e)–(f) Differences between colocated ML predictions and OE retrievals, and their respective error estimates.

https://doi.org/10.5194/egusphere-2025-4864
Preprint. Discussion started: 7 October 2025
© Author(s) 2025. CC BY 4.0 License.

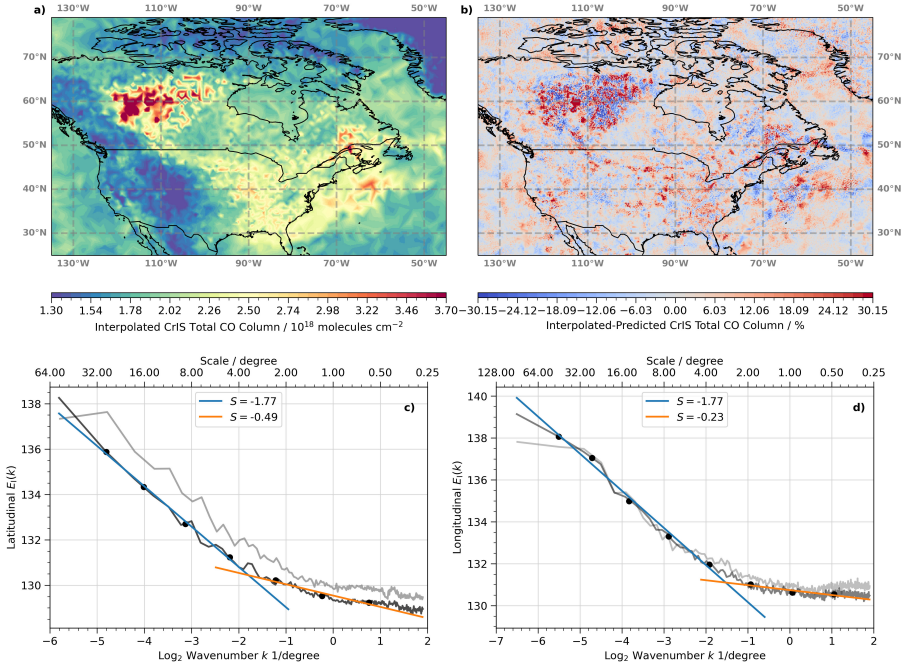

Figure 4. (a) Interpolated TROPESS total column CO on 10 June 2023. (b) Difference between interpolated and predicted CO. (c)–(d) Average power spectral density $E_{\mathrm{I}}(k)$ (black) as a function of wavenumber k for CO in latitudinal and longitudinal direction; $E_{\mathrm{I}}(k)$ for radiances at $2183.125\,\mathrm{cm}^{-1}$ are shown in gray. Blue and orange lines indicate linear fits through different regions of $E_{\mathrm{I}}(k)$.

on a similar but irregular grid, nearest-neighbor interpolation was used to retain most of the native variability. For comparison, linear and cubic spline interpolations were also evaluated.

Figure 4a shows the interpolated OE CO retrievals. This field appears significantly smoother than the ML predictions (Fig. 3c, especially for the region of enhanced CO over Western Canada and the Northeastern United States. The difference between the interpolated and predicted CO concentrations is illustrated in Fig. 4b, where blue and red colors indicate underestimation and overestimation by the interpolation, respectively. Deviations are centered around 0.50% but can exceed $\pm 30\%$, especially in areas of enhanced CO. Maximum differences increase further, to $\pm 48\%$ and $\pm 58\%$, when using nearest–neighbor or cubic spline interpolation, respectively.

To quantify the spatial variability in predicted CO over the whole scene, we calculate power spectral densities $E_{\mathrm{I}}(k)$, which describe how variance in a spatial signal is distributed across different wavenumbers (k). Many geophysical fields exhibit scale–invariant behavior over a large range of wavenumbers, with $E_{\mathrm{I}}(k)$ following a power law:

$$E_{\mathrm{I}}(k) \sim k^{-\beta}. \tag{1}$$

Sudden cahnges in the slope β, so–called scale breaks, indicate changes in the physical processes governing variability. Such breaks have been reported in cloud–reflected radiances (e.g., Davis et al., 1997), paleotemperature records (e.g., Nilsen

https://doi.org/10.5194/egusphere-2025-4864
Preprint. Discussion started: 7 October 2025
© Author(s) 2025. CC BY 4.0 License.

et al., 2016), and climate variability (e.g., Franzke et al., 2020). We compute $E_{\mathrm{I}}(k)$ as the squared amplitude of the Fourier–transformed CO predictions in both latitudinal and longitudinal directions.

Figures 4c–d present $E_{\mathrm{I}}(k)$ averaged over all grid points in latitude and longitude, respectively. A scale break is observed at $k \approx -1.70$, corresponding to spatial scales of ≈ 3.0–$3.5°$, in both directions. Linear fits before and after the break, shown in blue and orange, were computed using the octave binning method reported in Davis et al. (1996), which mitigates noise and limits energy accumulation at small scales. The binned $E_{\mathrm{I}}(k)$ values are plotted as black dots. At the scale break, the slope in latitude (longitude) flattens from $\beta \approx -1.77$ (-1.77) to $\beta \approx -0.49$ (-0.23), indicating a sharp increase in small–scale CO variability. This feature is associated with the de–correlation length scale of CO (not shown) and is likely linked to mesoscale atmospheric processes that merit further study. Notably, no secondary break is observed at smaller scales. In particular, no steeper $E_{\mathrm{I}}(k)$ decline is found below the operational TROPESS retrieval resolution, which would imply less variability and a smoother distribution. Instead, the CO field remains highly variable down to the Nyquist limit of $2 \cdot 0.80°/6 \approx 0.267°$.

Importantly, the observed scale break is neither an artifact of the retrieval nor dependent to the interpolation scheme. Applying the same analysis to CO–sensitive radiances in the spectral microwindow used in the OE retrieval (gray line in Figs. 4c–d) yields similar results: comparable scale breaks at $k \approx -2$ and consistent β values. Changing the interpolation scheme from nearest neighbor to linear or cubic spline has minimal effect on the location of the break, though β values increase slightly, reflecting increased variability across all scales. These minimal changes are not surprising, since the ML data are available at a very high spatial resolution (albeit on an irregular spatial grid).

In summary, the results in this section demonstrate that significant variability in total CO concentrations exists at scales below $\approx 4°$, and importantly, below the nominal $0.80°$ resolution of the TROPESS retrievals. The ML model allows this finer–scale variability to be resolved.

4.3 Computational costs

A key advantage of applying machine learning models in inference mode is their computational efficiency (Werner et al., 2023). As expected, the ML model is able to process a full day of CrIS radiance observations with remarkable speed. For 10 June 2023, the OE algorithm generated 44,192 CO column retrievals in ≈ 160 minutes. In contrast, the ML model predicted CO concentrations and associated diagnostics for 2,916,000 columns in just ≈ 6 minutes.

This performance difference is even more striking when considering the computational resources used. The OE algorithm was run on 60 compute nodes utilizing a total of 480 CPU cores, while the ML model required only a single compute node with 8 CPU cores. Additionally, the prediction success rate was higher: 98.4% for the ML model (based on a conservative outlier flag) compared to 90.69% for the OE retrievals.

The superior computational performance of the ML model ensures that every individual CrIS sample can be processed efficiently, enabling predictions for any species included in the TROPESS retrieval framework. Moreover, this efficiency opens the door to near–real–time applications and provides a practical means to use the ML outputs to help constrain or enhance OE retrievals (see the discussion in Sect. 5).

https://doi.org/10.5194/egusphere-2025-4864
Preprint. Discussion started: 7 October 2025
© Author(s) 2025. CC BY 4.0 License.

Note, however, that the OE algorithm produces a vertical profile and an associated averaging kernel matrix whereas the TROPESS–HYREF only predicts the derived column.

5 Conclusions

This study presents a novel fusion of physics–based optimal estimation (OE) retrievals and machine learning (ML) to produce predictions of global, high–resolution carbon monoxide (CO) concentrations and associated diagnostics from CrIS observations. Our approach leverages the strength of the TROPESS OE retrievals, namely accuracy, physical consistency, and interpretability, while using an artificial neural network to overcome their main limitation: sparse spatial sampling due to high computational costs and strict quality filtering. This enables us to increase the fraction of processed CrIS observations from $\approx 1\%$ to 100%.

The trained ML model within this MAchine Learning-OPtimal Estimation (TROPESS–HYREF) framework reproduces TROPESS CO column retrievals with high accuracy, achieving correlations exceeding 0.99 and low absolute biases $< 0.1\%$ across both test and validation data sets. Importantly, TROPESS–HYREF not only predicts columns concentrations, but also associated diagnostics, including column averaging kernels, degrees of freedom (DoF), and retrieval errors. This added information is crucial for proper scientific use of the predicted fields, enabling traceable comparisons with other satellite products, in situ data, model simulations, and ingestion into chemical data assimilation.

Using representative example scenes, we demonstrate that the TROPESS–HYREF predictions resolve fine–scale spatial structures and outperform standard interpolation methods, particularly in areas with elevated CO due to wildfire emissions. A scale analysis reveals significant spatial variability in the CO fields below $3.5°$ and, more importantly, below the OE retrieval's native $0.80°$ resolution, indicating that the ML predictions are resolving meaningful sub–retrieval–scale features. Notably, variability persists down to the Nyquist sampling limit imposed by the CrIS observation footprint.

In terms of computational performance, TROPESS–HYREF is able to process a full day of CrIS observations more than 25 times faster than the OE algorithm, despite producing predictions for over 65 times more observations (i.e., 1,625 times faster). The high success rate of the ML inference ($\approx 98.4\%$) compared to the OE retrieval ($\approx 90.7\%$) further ensures consistent, global data availability.

By providing retrieval–like products at full coverage and enhanced resolution, this work bridges the gap between physically constrained atmospheric retrievals and scalable machine learning predictions. The ML outputs are suitable for downstream applications, including data assimilation, model validation, and trend analysis. They also offer the potential to inform and constrain future retrieval efforts, e.g., using predictions as a prior states or as an additional quality flag, where large discrepancies between OE and ML results could highlight potential issues with individual samples. In addition, ML can continuously train on the operationally OE record as it expands in time. This enables TROPESS–HYREF to capture changes in atmospheric composition that might be lost with a stagnant training set. This fusion framework thus represents a significant step toward operational, physically consistent, high–resolution atmospheric composition products.

https://doi.org/10.5194/egusphere-2025-4864
Preprint. Discussion started: 7 October 2025
© Author(s) 2025. CC BY 4.0 License.

The methodology used for CO can be readily applied to all other trace gases retrieved by the TROPESS MUSES OE algorithm including ammonia (NH_3), ozone (O_3), and methane (CH_4). In addition, this approach can be extended to other instruments including TES, AIRS, OMI, and TROPOMI and their combinations such as CrIS+TROPOMI or AIRS+OMI (Fu et al., 2018; Malina et al., 2024). These efforts will enable a suite of full–coverage, physically informed ML products across multiple atmospheric constituents. In parallel, we are developing methods to use the ML predictions as a first guess in the OE retrieval algorithm. This hybrid approach promises to accelerate convergence, reduce computational costs, and potentially improve retrieval accuracy by providing physically realistic a priori estimates tailored to each CrIS observation. Together, these advances aim to enhance both the scalability and scientific value of satellite trace gas observations.

Code and data availability. CrIS L1B radiances and the TROPESS CO product files can be downloaded from GES DISC. A Zenodo repository (Werner et al., 2025) contains the HYREF CO model and all necessary Python routines, as well as a Jupyter notebook with step-by-step instructions, so interested parties can produce their own CO predictions. This repository also includes Jupyter notebooks, Python routines, and ancillary data sets to reproduce each figure in the manuscript.

Author contributions. FW, KWB, SL, JLL, VHP, and JLM have shaped the concept of this study and refined the approach during extensive discussions. FW, SL, and JLM implemented the ML algorithm into the current TROPESS algorithm pipeline. FW carried out the data analysis and prepared the figures for the manuscript. FW wrote the initial draft of the manuscript, which was subsequently refined by all authors.

Competing interests. The authors declare that they have no conflict of interest.

Acknowledgements. Government sponsorship acknowledged. Work at the Jet Propulsion Laboratory, California Institute of Technology, was carried out under contract with the National Aeronautics and Space Administration (80NM0018D0004).

https://doi.org/10.5194/egusphere-2025-4864
Preprint. Discussion started: 7 October 2025
© Author(s) 2025. CC BY 4.0 License.

References

Abadi, M., Agarwal, A., Barham, P., Brevdo, E., Chen, Z., Citro, C., Corrado, G. S., Davis, A., Dean, J., Devin, M., Ghemawat, S., Goodfellow, I., Harp, A., Irving, G., Isard, M., Jia, Y., Jozefowicz, R., Kaiser, L., Kudlur, M., Levenberg, J., Mane, D., Monga, R., Moore, S., Murray, D., Olah, C., Schuster, M., Shlens, J., Steiner, B., Sutskever, I., Talwar, K., Tucker, P., Vanhoucke, V., Vasudevan, V., Viegas, F., Vinyals, O., Warden, P., Wattenberg, M., Wicke, M., Yu, Y., and Zheng, X.: TensorFlow: Large-Scale Machine Learning on Heterogeneous Distributed Systems, arXiv [preprint], arxiv:1603.04467v2, 2016.

Aumann, H., Chahine, M., Gautier, C., Goldberg, M., Kalnay, E., McMillin, L., Revercomb, H., Rosenkranz, P., Smith, W., Staelin, D., Strow, L., and Susskind, J.: AIRS/AMSU/HSB on the Aqua mission: design, science objectives, data products, and processing systems, IEEE Trans. Geosci. Remote Sens., 41, 253–264, https://doi.org/10.1109/TGRS.2002.808356, 2003.

Beer, R., Glavich, T. A., and Rider, D. M.: Tropospheric emission spectrometer for the Earth Observing System's Aura satellite, Appl. Opt., 40, 2356–2367, https://doi.org/10.1364/AO.40.002356, 2001.

Bowman, K. and Henze, D. K.: Attribution of direct ozone radiative forcing to spatially resolved emissions, Geophysical Research Letters, 39, https://doi.org/https://doi.org/10.1029/2012GL053274, 2012.

Bowman, K., Rodgers, C., Kulawik, S., Worden, J., Sarkissian, E., Osterman, G., Steck, T., Lou, M., Eldering, A., Shephard, M., Worden, H., Lampel, M., Clough, S., Brown, P., Rinsland, C., Gunson, M., and Beer, R.: Tropospheric emission spectrometer: retrieval method and error analysis, IEEE Transactions on Geoscience and Remote Sensing, 44, 1297–1307, https://doi.org/10.1109/TGRS.2006.871234, 2006.

Bowman, K. W.: TROPESS CrIS-JPSS1 L2 Carbon Monoxide for Forward Stream, Summary Product V1, https://doi.org/10.5067/JL1HT3NGEAW3, 2021.

Buchholz, R. R., Hammerling, D., Worden, H. M., Deeter, M. N., Emmons, L. K., Edwards, D. P., and Monks, S. A.: Links Between Carbon Monoxide and Climate Indices for the Southern Hemisphere and Tropical Fire Regions, Journal of Geophysical Research: Atmospheres, 123, 9786–9800, https://doi.org/https://doi.org/10.1029/2018JD028438, 2018.

Buchholz, R. R., Worden, H. M., Park, M., Francis, G., Deeter, M. N., Edwards, D. P., Emmons, L. K., Gaubert, B., Gille, J., Martínez-Alonso, S., Tang, W., Kumar, R., Drummond, J. R., Clerbaux, C., George, M., Coheur, P.-F., Hurtmans, D., Bowman, K. W., Luo, M., Payne, V. H., Worden, J. R., Chin, M., Levy, R. C., Warner, J., Wei, Z., and Kulawik, S. S.: Air pollution trends measured from Terra: CO and AOD over industrial, fire-prone, and background regions, Remote Sensing of Environment, 256, 112 275, https://doi.org/https://doi.org/10.1016/j.rse.2020.112275, 2021.

Byrne, B., Liu, J., Lee, M., Yin, Y., Bowman, K. W., Miyazaki, K., Norton, A. J., Joiner, J., Pollard, D. F., Griffith, D. W. T., Velazco, V. A., Deutscher, N. M., Jones, N. B., and Paton-Walsh, C.: The Carbon Cycle of Southeast Australia During 2019–2020: Drought, Fires, and Subsequent Recovery, AGU Advances, 2, e2021AV000 469, https://doi.org/https://doi.org/10.1029/2021AV000469, e2021AV000469 2021AV000469, 2021.

Byrne, B., Liu, J., Bowman, K. W., Pascolini-Campbell, M., Chatterjee, A., Pandey, S., Miyazaki, K., van der Werf, G. R., Wunch, D., Wennberg, P. O., Roehl, C. M., and Sinha, S.: Carbon emissions from the 2023 Canadian wildfires, Nature, 633, 835–839, https://doi.org/10.1038/s41586-024-07878-z, 2024.

Chollet, F. et al.: Keras, https://keras.io, 2015.

https://doi.org/10.5194/egusphere-2025-4864
Preprint. Discussion started: 7 October 2025
© Author(s) 2025. CC BY 4.0 License.

Clerbaux, C., Hadji-Lazaro, J., Payan, S., Camy-Peyret, C., Wang, J., Edwards, D. P., and Luo, M.: Retrieval of CO from nadir remote-sensing measurements in the infrared by use of four different inversion algorithms, Appl. Opt., 41, 7068–7078, https://doi.org/10.1364/AO.41.007068, 2002.

Clerbaux, C., Boynard, A., Clarisse, L., George, M., Hadji-Lazaro, J., Herbin, H., Hurtmans, D., Pommier, M., Razavi, A., Turquety, S., Wespes, C., and Coheur, P.-F.: Monitoring of atmospheric composition using the thermal infrared IASI/MetOp sounder, Atmospheric Chemistry and Physics, 9, 6041–6054, https://doi.org/10.5194/acp-9-6041-2009, 2009.

Davis, A., Marshak, A., Wiscombe, W., and Cahalan, R.: Scale invariance of liquid water distributions in marine stratocumulus. Part I: Spectral properties and stationarity issues, J. Atmos. Sci., 53, 1538–1558, https://doi.org/10.1175/1520-0469(1996)053<1538:SIOLWD>2.0.CO;2, 1996.

Davis, A., Marshak, A., Cahalan, R., and Wiscombe, W.: The Landsat scale break in stratocumulus as a three-dimensional radiative transfer effect: Implications for cloud remote sensing, J. Atmos. Sci., 54, 241–260, 1997.

Drummond, J. R., Zou, J., Nichitiu, F., Kar, J., Deschambaut, R., and Hackett, J.: A review of 9-year performance and operation of the MOPITT instrument, Advances in Space Research, 45, 760–774, https://doi.org/https://doi.org/10.1016/j.asr.2009.11.019, 2010.

Edwards, D. P., Emmons, L. K., Hauglustaine, D. A., Chu, D. A., Gille, J. C., Kaufman, Y. J., Pétron, G., Yurganov, L. N., Giglio, L., Deeter, M. N., Yudin, V., Ziskin, D. C., Warner, J., Lamarque, J.-F., Francis, G. L., Ho, S. P., Mao, D., Chen, J., Grechko, E. I., and Drummond, J. R.: Observations of carbon monoxide and aerosols from the Terra satellite: Northern Hemisphere variability, Journal of Geophysical Research: Atmospheres, 109, https://doi.org/https://doi.org/10.1029/2004JD004727, 2004.

Field, R. D., Luo, M., Kim, D., Del Genio, A. D., Voulgarakis, A., and Worden, J.: Sensitivity of simulated tropospheric CO to subgrid physics parameterization: A case study of Indonesian biomass burning emissions in 2006, Journal of Geophysical Research: Atmospheres, 120, 11,743–11,759, https://doi.org/https://doi.org/10.1002/2015JD023402, 2015.

Field, R. D., Luo, M., Fromm, M., Voulgarakis, A., Mangeon, S., and Worden, J.: Simulating the Black Saturday 2009 smoke plume with an interactive composition-climate model: Sensitivity to emissions amount, timing, and injection height, Journal of Geophysical Research: Atmospheres, 121, 4296–4316, https://doi.org/https://doi.org/10.1002/2015JD024343, 2016.

Franzke, C. L. E., Barbosa, S., Blender, R., Fredriksen, H.-B., Laepple, T., Lambert, F., Nilsen, T., Rypdal, K., Rypdal, M., Scotto, M. G., Vannitsem, S., Watkins, N. W., Yang, L., and Yuan, N.: The Structure of Climate Variability Across Scales, Reviews of Geophysics, 58, e2019RG000 657, https://doi.org/https://doi.org/10.1029/2019RG000657, e2019RG000657 10.1029/2019RG000657, 2020.

Fu, D., Bowman, K. W., Worden, H. M., Natraj, V., Worden, J. R., Yu, S., Veefkind, P., Aben, I., Landgraf, J., Strow, L., and Han, Y.: High-resolution tropospheric carbon monoxide profiles retrieved from CrIS and TROPOMI, Atmospheric Measurement Techniques, 9, 2567–2579, https://doi.org/10.5194/amt-9-2567-2016, 2016.

Fu, D., Kulawik, S. S., Miyazaki, K., Bowman, K. W., Worden, J. R., Eldering, A., Livesey, N. J., Teixeira, J., Irion, F. W., Herman, R. L., Osterman, G. B., Liu, X., Levelt, P. F., Thompson, A. M., and Luo, M.: Retrievals of tropospheric ozone profiles from the synergism of AIRS and OMI: methodology and validation, Atmospheric Measurement Techniques, 11, 5587–5605, https://doi.org/10.5194/amt-11-5587-2018, 2018.

Fu, D., Millet, D. B., Wells, K. C., Payne, V. H., Yu, S., Guenther, A., and Eldering, A.: Direct retrieval of isoprene from satellite-based infrared measurements, Nature Communications, 10, 3811, https://doi.org/10.1038/s41467-019-11835-0, 2019.

Gaubert, B., Worden, H. M., Arellano, A. F. J., Emmons, L. K., Tilmes, S., Barré, J., Martinez Alonso, S., Vitt, F., Anderson, J. L., Alkemade, F., Houweling, S., and Edwards, D. P.: Chemical Feedback From Decreasing Carbon Monoxide Emissions, Geophysical Research Letters, 44, 9985–9995, https://doi.org/https://doi.org/10.1002/2017GL074987, 2017.

https://doi.org/10.5194/egusphere-2025-4864
Preprint. Discussion started: 7 October 2025
© Author(s) 2025. CC BY 4.0 License.

Goodfellow, I., Bengio, Y., and Courville, A.: Deep Learning (Adaptive Computation and Machine Learning series), The MIT Press, Cambridge, MA, 2016.

Grivas, G. and Chaloulakou, A.: Artificial neural network models for prediction of PM10 hourly concentrations, in the Greater Area of Athens, Greece, Atmospheric Environment, 40, 1216–1229, https://doi.org/10.1016/j.atmosenv.2005.10.036, 2006.

Han, Y., Revercomb, H., Cromp, M., Gu, D., Johnson, D., Mooney, D., Scott, D., Strow, L., Bingham, G., Borg, L., Chen, Y., DeSlover, D., Esplin, M., Hagan, D., Jin, X., Knuteson, R., Motteler, H., Predina, J., Suwinski, L., Taylor, J., Tobin, D., Tremblay, D., Wang, C., Wang, L., Wang, L., and Zavyalov, V.: Suomi NPP CrIS measurements, sensor data record algorithm, calibration and validation activities, and record data quality, Journal of Geophysical Research: Atmospheres, 118, 12,734–12,748, https://doi.org/https://doi.org/10.1002/2013JD020344, 2013.

Holloway, T., Levy II, H., and Kasibhatla, P.: Global distribution of carbon monoxide, Journal of Geophysical Research: Atmospheres, 105, 12 123–12 147, https://doi.org/https://doi.org/10.1029/1999JD901173, 2000.

IPCC: Climate Change 2023: Synthesis Report. A Report of the Intergovernmental Panel on Climate Change, IPCC, https://doi.org/10.59327/IPCC/AR6-9789291691647, 2023.

Jacob, D.: Instroduction to Atmospheric Chemistry, vol. ISBN 9780691001852, Princeton University Press, 1999.

Jain, P., Barber, Q. E., Taylor, S. W., Whitman, E., Castellanos Acuna, D., Boulanger, Y., Chavardès, R. D., Chen, J., Englefield, P., Flannigan, M., Girardin, M. P., Hanes, C. C., Little, J., Morrison, K., Skakun, R. S., Thompson, D. K., Wang, X., and Parisien, M.-A.: Drivers and Impacts of the Record-Breaking 2023 Wildfire Season in Canada, Nature Communications, 15, 6764, https://doi.org/10.1038/s41467-024-51154-7, 2024.

Jones, D. B. A., Bowman, K. W., Palmer, P. I., Worden, J. R., Jacob, D. J., Hoffman, R. N., Bey, I., and Yantosca, R. M.: Potential of observations from the Tropospheric Emission Spectrometer to constrain continental sources of carbon monoxide, Journal of Geophysical Research: Atmospheres, 108, https://doi.org/https://doi.org/10.1029/2003JD003702, 2003.

Lelieveld, J., Gromov, S., Pozzer, A., and Taraborrelli, D.: Global tropospheric hydroxyl distribution, budget and reactivity, Atmospheric Chemistry and Physics, 16, 12 477–12 493, https://doi.org/10.5194/acp-16-12477-2016, 2016.

Luo, M., Worden, H. M., Field, R. D., Tsigaridis, K., and Elsaesser, G. S.: TROPESS-CrIS CO single-pixel vertical profiles: intercomparisons with MOPITT and model simulations for 2020 western US wildfires, Atmospheric Measurement Techniques, 17, 2611–2624, https://doi.org/10.5194/amt-17-2611-2024, 2024.

Malina, E., Bowman, K. W., Kantchev, V., Kuai, L., Kurosu, T. P., Miyazaki, K., Natraj, V., Osterman, G. B., Oyafuso, F., and Thill, M. D.: Joint spectral retrievals of ozone with Suomi NPP CrIS augmented by S5P/TROPOMI, Atmospheric Measurement Techniques, 17, 5341–5371, https://doi.org/10.5194/amt-17-5341-2024, 2024.

Miyazaki, K., Eskes, H. J., and Sudo, K.: A tropospheric chemistry reanalysis for the years 2005–2012 based on an assimilation of OMI, MLS, TES, and MOPITT satellite data, Atmospheric Chemistry and Physics, 15, 8315–8348, https://doi.org/10.5194/acp-15-8315-2015, 2015.

Neyra-Nazarrett, O. A., Miyazaki, K., Bowman, K. W., and Saide, P. E.: An Assessment of TROPESS CrIS and TROPOMI CO Retrievals and Their Synergies for the 2020 Western U.S. Wildfires, Remote Sensing, 17, https://doi.org/10.3390/rs17111854, 2025.

Nilsen, T., Rypdal, K., and Fredriksen, H.-B.: Are there multiple scaling regimes in Holocene temperature records?, Earth System Dynamics, 7, 419–439, https://doi.org/10.5194/esd-7-419-2016, 2016.

Noël, S., Reuter, M., Buchwitz, M., Borchardt, J., Hilker, M., Schneising, O., Bovensmann, H., Burrows, J. P., Di Noia, A., Parker, R. J., Suto, H., Yoshida, Y., Buschmann, M., Deutscher, N. M., Feist, D. G., Griffith, D. W. T., Hase, F., Kivi, R., Liu, C., Morino, I., Notholt, J.,

https://doi.org/10.5194/egusphere-2025-4864
Preprint. Discussion started: 7 October 2025
© Author(s) 2025. CC BY 4.0 License.

Oh, Y.-S., Ohyama, H., Petri, C., Pollard, D. F., Rettinger, M., Roehl, C., Rousogenous, C., Sha, M. K., Shiomi, K., Strong, K., Sussmann, R., Té, Y., Velazco, V. A., Vrekoussis, M., and Warneke, T.: Retrieval of greenhouse gases from GOSAT and GOSAT-2 using the FOCAL algorithm, Atmospheric Measurement Techniques, 15, 3401–3437, https://doi.org/10.5194/amt-15-3401-2022, 2022.

Reed, R. and Marks, ll, R. J.: Neural Smithing: Supervised Learning in Feedforward Artificial Neural Networks, A Bradford Book, 1999.

Reichle Jr., H. G., Connors, V. S., Holland, J. A., Sherrill, R. T., Wallio, H. A., Casas, J. C., Condon, E. P., Gormsen, B. B., and Seiler, W.: The distribution of middle tropospheric carbon monoxide during early October 1984, Journal of Geophysical Research: Atmospheres, 95, 9845–9856, https://doi.org/https://doi.org/10.1029/JD095iD07p09845, 1990.

Rodgers, C.: Inverse Methods for Atmospheric Sounding, World Scientific Publishing Co., 2000.

Saponaro, G., Kolmonen, P., Karhunen, J., Tamminen, J., and de Leeuw, G.: A neural network algorithm for cloud fraction estimation using NASA-Aura OMI VIS radiance measurements, Atmospheric Measurement Techniques, 6, 2301–2309, https://doi.org/10.5194/amt-6-2301-2013, 2013.

Schultz, M. G., Akimoto, H., Bottenheim, J., Buchmann, B., Galbally, I. E., Gilge, S., Helmig, D., Koide, H., Lewis, A. C., Novelli, P. C., Plass-Dülmer, C., Ryerson, T. B., Steinbacher, M., Steinbrecher, R., Tarasova, O., Tørseth, K., Thouret, V., and Zellweger, C.: The Global Atmosphere Watch reactive gases measurement network, Elementa: Science of the Anthropocene, 3, 000 067, https://doi.org/10.12952/journal.elementa.000067, 2015.

Schultz, M. G., Betancourt, C., Gong, B., Kleinert, F., Langguth, M., Leufen, L. H., Mozaffari, A., and Stadtler, S.: Can deep learning beat numerical weather prediction?, Phil. Trans. R. Soc. A., 379, https://doi.org/10.1098/rsta.2020.0097, 2021.

Strode, S. A., Worden, H. M., Damon, M., Douglass, A. R., Duncan, B. N., Emmons, L. K., Lamarque, J.-F., Manyin, M., Oman, L. D., Rodriguez, J. M., Strahan, S. E., and Tilmes, S.: Interpreting space–based trends in carbon monoxide with multiple models, Atmospheric Chemistry and Physics, 16, 7285–7294, https://doi.org/10.5194/acp-16-7285-2016, 2016.

Tyralis, H. and Papacharalampous, G.: A review of predictive uncertainty estimation with machine learning, Artificial Intelligence Review, 57, 94, https://doi.org/10.1007/s10462-023-10698-8, 2024.

UW-Madison Space Science and Engineering Center: Hank Revercomb; UMBC Atmospheric Spectroscopy Laboratory: Larrabee Strow: JPSS-1 CrIS Level 1B Full Spectral Resolution V2, https://doi.org/10.5067/EETSCFBDBLX6, 2018.

Veefkind, J., Aben, I., McMullan, K., Förster, H., de Vries, J., Otter, G., Claas, J., Eskes, H., de Haan, J., Kleipool, Q., van Weele, M., Hasekamp, O., Hoogeveen, R., Landgraf, J., Snel, R., Tol, P., Ingmann, P., Voors, R., Kruizinga, B., Vink, R., Visser, H., and Levelt, P.: TROPOMI on the ESA Sentinel-5 Precursor: A GMES mission for global observations of the atmospheric composition for climate, air quality and ozone layer applications, Remote Sensing of Environment, 120, 70–83, https://doi.org/https://doi.org/10.1016/j.rse.2011.09.027, the Sentinel Missions - New Opportunities for Science, 2012.

von Clarmann, T. and Glatthor, N.: The application of mean averaging kernels to mean trace gas distributions, Atmospheric Measurement Techniques, 12, 5155–5160, https://doi.org/10.5194/amt-12-5155-2019, 2019.

Werner, F., Schwartz, M. J., Livesey, N. J., Read, W. G., and Santee, M. L.: Extreme Outliers in Lower Stratospheric Water Vapor Over North America Observed by MLS: Relation to Overshooting Convection Diagnosed From Colocated Aqua-MODIS Data, Geophysical Research Letters, 47, e2020GL090 131, https://doi.org/10.1029/2020GL090131, 2020.

Werner, F., Livesey, N. J., Schwartz, M. J., Read, W. G., Santee, M. L., and Wind, G.: Improved cloud detection for the Aura Microwave Limb Sounder (MLS): training an artificial neural network on colocated MLS and Aqua MODIS data, Atmos. Meas. Tech., 14, 7749–7773, https://doi.org/10.5194/amt-14-7749-2021, 2021.

https://doi.org/10.5194/egusphere-2025-4864
Preprint. Discussion started: 7 October 2025
© Author(s) 2025. CC BY 4.0 License.

Werner, F., Livesey, N. J., Millán, L. F., Read, W. G., Schwartz, M. J., Wagner, P. A., Daffer, W. H., Lambert, A., Tolstoff, S. N., and Santee, M. L.: Applying machine learning to improve the near-real-time products of the Aura Microwave Limb Sounder, Atmospheric Measurement Techniques, 16, 2733–2751, https://doi.org/10.5194/amt-16-2733-2023, 2023.

Werner, F., Bowman, K. W., Lee, S., Laughner, J. L., Payne, V. H., and McDuffie, J. L.: Zenodo repository for A hybrid optimal estimation and machine learning approach to predict atmospheric composition, *Zenodo*, https://doi.org/10.5281/zenodo.16968703, 2025.

Worden, H. M., Deeter, M. N., Frankenberg, C., George, M., Nichitiu, F., Worden, J., Aben, I., Bowman, K. W., Clerbaux, C., Coheur, P. F., de Laat, A. T. J., Detweiler, R., Drummond, J. R., Edwards, D. P., Gille, J. C., Hurtmans, D., Luo, M., Martínez-Alonso, S., Massie, S., Pfister, G., and Warner, J. X.: Decadal record of satellite carbon monoxide observations, Atmospheric Chemistry and Physics, 13, 837–850, https://doi.org/10.5194/acp-13-837-2013, 2013.

Worden, H. M., Francis, G. L., Kulawik, S. S., Bowman, K. W., Cady-Pereira, K., Fu, D., Hegarty, J. D., Kantchev, V., Luo, M., Payne, V. H., Worden, J. R., Commane, R., and McKain, K.: TROPESS/CrIS carbon monoxide profile validation with NOAA GML and ATom in situ aircraft observations, Atmospheric Measurement Techniques, 15, 5383–5398, https://doi.org/10.5194/amt-15-5383-2022, 2022.

Zeng, Z.-C., Lee, L., Qi, C., Clarisse, L., and Van Damme, M.: Optimal estimation retrieval of tropospheric ammonia from the Geostationary Interferometric Infrared Sounder on board FengYun-4B, Atmospheric Measurement Techniques, 16, 3693–3713, https://doi.org/10.5194/amt-16-3693-2023, 2023.

Zheng, B., Chevallier, F., Yin, Y., Ciais, P., Fortems-Cheiney, A., Deeter, M. N., Parker, R. J., Wang, Y., Worden, H. M., and Zhao, Y.: Global atmospheric carbon monoxide budget 2000–2017 inferred from multi-species atmospheric inversions, Earth System Science Data, 11, 1411–1436, https://doi.org/10.5194/essd-11-1411-2019, 2019.